Eur. Phys. J. E **24**, 331–341 (2007)
DOI 10.1140/epje/i2007-10244-x

THE EUROPEAN PHYSICAL JOURNAL E

Permeate flux inflection due to concentration polarization in crossflow membrane filtration: A novel analytic approach

A.S. Kim[a]

Civil and Environmental Engineering, University of Hawaii at Manoa, Honolulu, HI 96822, USA

Received 24 February 2007 and Received in final form 16 September 2007
Published online: 8 January 2008 –

Abstract. A convection-diffusion equation for membrane filtration is analytically solved assuming fast crossflow velocity of a simple shear flow tangential to the membrane surface. In the direction normal to the membrane surface, solute concentration varies in a partially exponential and partially power-wise manner. The permeate flux in an asymptotic limit is proportional to the inverse square root of the distance from the inlet of the membrane channel. Osmotic pressure due to retained solutes on the membrane surface controls the profile of the permeate flux, which undergoes an inflection along the tangential direction if applied pressure is more than four times the feed osmotic pressure.

PACS. 82.39.Wj Ion exchange, dialysis, osmosis, electro-osmosis, membrane processes

1 Introduction

Laminar flow tangential to a porous wall has received close attention in past decades because of its plethoric applications to, for example, bio-medical systems, diffusion processes, membrane separation, and so forth. A similarity solution method can be used to solve the Navier-Stokes equation for an incompressible viscous flow along a porous channel. Key findings are briefly summarized in the following paragraphs.

Berman [1] reduced the Navier-Stokes equation to a fourth-order non-linear ordinary differential equation, applied no-slip boundary conditions on two porous walls of a rectangular channel, and developed a perturbation solution as a series in small suction Reynolds number. Bundy and Weissberg [2] measured pressure drop and exit centerline velocity of a porous channel and showed good agreement of their experiments with Berman's theoretical prediction. Weissberg [3] used Morduchow's polynomial approximation method [4] and indicated that similarity solutions do not exist for high suction rates. Along the same lines, Brady [5] showed that at large Reynolds numbers, the flow everywhere in a finite but arbitrarily long, uniformly porous channel is influenced by the inlet condition. The similarity solution loses its validity if the critical Reynolds number of 2.3 is exceeded. Durlofsky and Brady [6] showed that the non-monotonic variation of the tangential velocity in the normal direction to the porous wall provides the spatial instability of the similarity solution.

[a] e-mail: albertsk@hawaii.edu

The no-slip boundary condition on the porous wall was presumed in the similarity solution approaches described above. The validity of the no-slip boundary condition is not clear when it is imposed on a porous interface with large open pores. Beaver and Joseph [7] suggested that the slip velocity is proportional to the velocity gradient above the porous wall. Taylor [8] showed the significance of a porous surface structure instead of channel geometry, and Jeong [9] investigated the slip boundary condition on an idealized porous wall. Recently, Chellam and Liu [10] investigated the necessary and sufficient conditions for the presence of Berman's similarity solution for slip flow and provided the slip parameter for ultrafiltration.

Fundamental studies on the flow over a porous surface can significantly contribute to accurate analyses and optimal design of pressure-driven membrane filtration processes such as microfiltration (MF), ultrafiltration (UF), nanofiltration (NF), and reverse osmosis (RO), which have been extensively used for separating particulate materials, macromolecules, organic matters, and salt ions. Filtration operations can be classified into dead-end and crossflow modes. In the dead-end filtration mode, feed solution flows normal to the membrane surface, and solutes are mostly retained on the membrane surface while the solvent passes through the membrane. Accumulation of solutes increases on the membrane surface with respect to time, and hence diminishes the permeate flux. In the crossflow mode (shown in Fig. 1), the feed stream is introduced tangentially to the membrane surface. Solvent passing across the membrane generates permeate flow while the remainder is flushed out as concentrate stream. Directions of the feed (tangential to the membrane surface) and

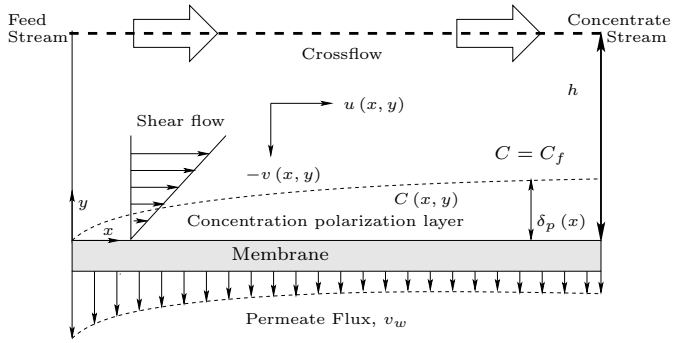

Fig. 1. Schematic of concentration polarization and permeate flux profiles during crossflow membrane filtration.

the permeate (normal to the membrane surface) are perpendicular to, *i.e.*, crossed over, each other. A quasi-steady state can be reached in this operational mode, in which the permeate flux is almost independent of the elapsed filtration time. The spatial bias of concentration normal to the membrane surface is defined as concentration polarization (CP). The solute concentration on the membrane surface, called wall concentration, is therefore (much) higher than that of the feed solution, hindering solvent transport through the membrane due to osmotic pressure. In this light, an in-depth understanding of CP is crucially important to optimize the membrane processes while the interfacial phenomenon is convolutely affected by applied pressure and imposed flow field.

Michaels [11] firstly developed a stagnant film theory wherein the permeate flux is logarithmically proportional to the ratio of the wall concentration to the feed concentration, especially when solute passage through the membrane is negligible (see Sect. 3.3). The proportionality constant, termed mass transfer coefficient, is often obtained using empirical correlations [12] due to the mathematical intricacy of governing mass balance equations. Detailed mathematical analyses of the stagnant film theory and an excellent review of CP can be found elsewhere [13,14]. Further theoretical development of CP phenomena can be classified into two categories: integral solution method (ISM) [15,16] and similarity solution method (SSM) [17, 18]. ISM assumes the power-wise dependence of the concentration profile along the normal direction to the membrane surface. The exponent of the power law is related to the boundary layer Peclet number [19]. SSM chooses a dimensionless transformation that makes the CP layer thickness proportional to the cube root of the distance from the channel inlet in the tangential direction. De *et al.* later combined the above two methods and provided a unified theory [20].

In the absence of slip flow, downward convection and upward diffusion of solutes are balanced on the membrane surface. This boundary condition was often assumed to be valid over the entire (thin) CP layer and hence was integrated across the boundary layer [21–23]. The continuity equation is incorporated into the convection-diffusion equation, and the excess concentration, *i.e.*, the actual concentration subtracted by feed concentration, is introduced for an excess mass balance [24,25]. In this light, Song and Elimelech [21] used the excess concentration to balance the convection and diffusion of solutes within the CP layer, and the validity of their approach can be found elsewhere [26].

Theoretical approaches (separately) focus on either the estimation of accurate flow fields in a porous channel or the evaluation of CP on the membrane surface. Mathematical complexity of the governing equations precludes further development of analytic solutions that can contribute to a holistic understanding of CP during crossflow filtration. It has been argued that the concentration varies in the normal direction following an exponential or power-wise decay form [19], while permeate velocity seems to decrease following a typical power law in the tangential direction [27]. Flow slip on the porous membrane surfaces is rarely investigated as it is negligible on RO/NF membrane surfaces [28].

Various solutions for CP depend on specific paths of theoretical derivations with chosen assumptions and approximations. A rigorous analytic solution that readily includes coupled behaviors of solute concentration and fluid flow near the membrane surface has not been reported yet. In this light, the current study considers a thin CP layer in a simple shear flow on the RO membrane surface and provides coupled analytic solutions for profiles of solute concentration and permeate velocity.

2 Theory

2.1 Governing equation

Figure 1 shows a schematic of crossflow membrane filtration, where the thin concentration polarization is emphasized as it undergoes a simple shear field over the membrane surface. Berman's similarity solution using the perturbation method provides a parabolic crossflow profile, which is in this study approximated as a linear shear flow in close proximity to the membrane surface. The mass balance equation for crossflow membrane filtration in a steady state is represented as

$$\frac{\partial}{\partial x}\left(D\frac{\partial C}{\partial x} - uC\right) + \frac{\partial}{\partial y}\left(D\frac{\partial C}{\partial y} - vC\right) = 0, \quad (1)$$

where u and v are components of the flow field in the tangential (x) and normal (y) directions, respectively, and C is the solute number concentration.

In this study, the concentration-dependent solute diffusivity D is approximated as a constant bulk diffusivity D_0, *i.e.*,

$$D(C) \approx D_0\,. \quad (2)$$

A constant diffusivity indicates that the osmotic pressure linearly increases with the solute concentration, which is the case in the Van 't Hoff equation for a dilute concentration (*e.g.*, see Eq. (51)). When interactions between solutes are additive pair-wise, the equilibrium distribution function is often used to calculate viral coefficients

of the pressure [29]. The nonlinearity of the osmotic pressure with respect to the solute concentration procreates the concentration-dependent diffusivity [30], which is important when solutes undergo strong mutual interactions, and/or the concentration is very high and even close to a critical point of liquid-solid phase transtion. In membrane filtration, especially in RO and NF of seawater and brackish water desalination, however, feed ion concentrations range from 0.1 to 1.0 M, and wall concentrations are as much as 2 or 3 times higher than those due to the concentration polarization. In these cases, the Van 't Hoff equation provides a good estimation of the osmotic pressure and validiates the approximation of equation (2).

The diffusion in the tangential direction is assumed to be negligible relative to the other three terms including convection in the same direction [13,17,18,24,31,32]:

$$\frac{D_0 \frac{\partial C}{\partial x}}{uC} = O\left(\frac{D_0 \Delta C}{L}\frac{1}{\bar{u}\bar{C}}\right) \approx O\left(\frac{D_0}{L\bar{u}}\right) \ll 1, \qquad (3)$$

where L is the length the membrane channel, $\bar{u}$ is the average crossflow velocity, $\bar{C}$ is the average concentration within the membrane channel, and ΔC is the concentration difference between the concentrate and feed. The ratio of ΔC to $\bar{C}$ within the CP layer is of an order of $O(1)$ unless low pressure drives negligible permeate flux and hence minimal concentration polarization. Typical values of D_0, L, and $\bar{u}$ are on the orders of $O(10^{-9})\,\mathrm{m}^2/\mathrm{s}$, $O(10^{-1})\,\mathrm{m}$, and $O(10^{-1})\,\mathrm{m/s}$, respectively so that the approximation of equation (3) is reasonable. An asymptotic analysis of neglecting the tangential diffusion using the formal expansion is in Appendix A.

Considering a thin CP layer, whose thickness δ_p is presumed to be (much) smaller than the half height h, further approximations are possible:

$$v(x,y) \cong -v_w(x)\left(1 - \frac{\gamma_0}{2\bar{u}\cdot 2h}y^2\right), \qquad (4)$$

where the negative sign indicates the downward magnitude of the permeate velocity v_w, and

$$u(x,y) \cong \gamma(x)y = \gamma_0\left(1 - \frac{1}{\bar{u}\cdot 2h}\int_0^x v_w(x')\mathrm{d}x'\right)y, \quad \text{for } y \le \delta_p\,, \qquad (5)$$

where $\gamma_0 (= 3\bar{u}/h)$ is a constant wall shear rate for a rectangular channel. The second terms[1] inside the parentheses of equations (4) and (5), as small perturbations, indicate, respectively, that v reaches its maximum on the membrane surface, and the local shear rate $\gamma(x)$ varies along the tangential direction due to the solvent mass balance. From equations (4) and (5) the continuity equation is satisfied, showing zero divergence of the flow field, such as

$$\frac{\partial u}{\partial x} + \frac{\partial v}{\partial y} = 0. \qquad (6)$$

[1] In equations (4) and (5), $2h$ is replaced by h if two identical membranes were located at $y = 0$ and $y = 2h$ [1].

At (and above) the CP layer boundary (*i.e.*, $y = \delta_p$), the concentration is set equal to the feed concentration C_f, *i.e.*,

$$C(x, y = \delta_p) = C_f\,, \qquad (7)$$

as illustrated in Figure 1. Above the CP layer, the concentration is kept constant due to the continuous supply of solutes from the feed solution flowing with velocity of u.

Nondimensionalization of equation (1) with equations (4) and (5) yields

$$\eta\,\frac{\partial}{\partial\xi}\left(\phi - \phi\alpha\Omega(\xi)\right) = N_D\left(\frac{\partial^2\phi}{\partial\eta^2} + \mathrm{Pe}\,\omega(\xi)\frac{\partial}{\partial\eta}\left[\phi - \phi\frac{3}{4}\eta^2\right]\right), \qquad (8)$$

where

$$\xi = \frac{x}{L}\,, \qquad (9)$$

$$\eta = \frac{y}{h}\,, \qquad (10)$$

$$\omega(\xi) = \frac{v_w(x)}{v_{w0}}\,, \qquad (11)$$

$$\phi = \frac{C}{C_f}\,, \qquad (12)$$

$$N_D = \frac{D_0 L}{\gamma_0 h^3}\,, \qquad (13)$$

$$\alpha = \frac{v_{w0}L}{2\bar{u}h}\,, \qquad (14)$$

$$\mathrm{Pe} = \frac{v_{w0}h}{D_0}\,. \qquad (15)$$

Here, ϕ is the dimensionless solute concentration, v_{w0} is the permeate flux at the inlet of the membrane channel (*i.e.*, $x = 0$) (see Eq. (53)), α is a ratio of permeate to crossflow rate, and Pe is the Peclet number. Equation (10) uses h as a characteristic length to nondimensionalize the normal coordinate y. SSM scales y in terms of δ_p, which requires the pre-determined functional form of $\delta_p \sim \xi^{1/3}$ [17, 18]. Although the transformation used in SSM provides a mathematical convenience, it only calculates the permeate flux as a response to the pre-set δ_p so that the feedback convolution between convection and diffusion cannot be rigorously investigated. The dimensionless, length-averaged permeate flux Ω is defined as

$$\Omega(\xi) = \int_0^\xi \omega(\xi')\mathrm{d}\xi'\,, \qquad (16)$$

which is an integration of the dimensionless permeate flux from the inlet to the outlet of the membrane channel in a scaled x-coordinate.

Now, a simple functional transformation is performed using

$$q = \exp\left[-\frac{v_w y}{D_0}\right] = \exp\left[-\mathrm{Pe}\,\omega(\xi)\eta\right] \qquad (17)$$

and hence

$$\frac{\partial\phi}{\partial\eta} = \frac{\partial q}{\partial\eta}\frac{\partial\phi}{\partial q} = -\,\mathrm{Pe}\,\omega(\xi) q\frac{\partial\phi}{\partial q}\,, \tag{18}$$

$$\frac{\partial^2\phi}{\partial\eta^2} = \mathrm{Pe}^2\,\omega^2(\xi)\left(q^2\frac{\partial^2\phi}{\partial q^2} + q\frac{\partial\phi}{\partial q}\right). \tag{19}$$

Equations (18) and (19) greatly simplify equation (8) after dropping terms with α and η^2

$$\frac{1}{K\omega^3}\frac{\partial\phi}{\partial\xi} = -\frac{q^2}{\ln q}\frac{\partial^2\phi}{\partial q^2}\,, \tag{20}$$

where

$$K = \frac{L v_{w0}^3}{\gamma_0 D_0^2}\,, \tag{21}$$

which is a dimensionless number mathematically derived by this analysis. The term with α is ignored due to the fast crossflow velocity. The typical values of v_{w0} and $\bar{u}$ are of the order of $O(10^{-6}$–$10^{-5})$ m/s and $O(10^{-1}$–$10^{0})$ m/s, respectively. The ratio of v_{w0} to $\bar{u}$ varies from 10^{-6} to 10^{-4}. Therefore, unless the length is more than about 1000 times greater than the height, the condition of negligible α is valid in most cases. The thickness of the thin CP layer is typically a few percent of the channel (half) height (see Fig. 3 for example). Therefore, neglecting η^2 in equation (8) would not provide noticeable errors in this approximation. Consequently equation (20) encompasses the approximated flow field, which satisfies the continuity equation at an unperturbed level:

$$\frac{\partial(\gamma_0 y)}{\partial x} + \frac{\partial(-v_w(x))}{\partial y} = 0. \tag{22}$$

Typically, RO/NF membrane modules have channel height (or radius) on the order of millimeters. In these cases, the suction Reynolds number defined as

$$\mathrm{Re}_{\mathrm{suction}} = \frac{v_{w0} h}{\nu}\,, \tag{23}$$

where ν is the kinematic viscosity, is much smaller than 1, and the crossflow Reynolds number defined as

$$\mathrm{Re}_{\mathrm{cross}} = \frac{\bar{u} h}{\nu} \tag{24}$$

is of the order of $O(10^2)$. The two Reynolds numbers therefore indicate that RO and NF filtration processes are within a stable range of Berman's similarity solution for the viscous laminar flow [1].

2.2 Separation of variables

Using the method of separation of variables, a specific form of a solution for ϕ is suggested as follows:

$$\phi(\xi, q) = X(\xi)Q(q), \tag{25}$$

where X and Q are sole functions of ξ and q, respectively. Therefore, substituting equation (25) into equation (20) yields

$$\frac{1}{K\omega^3}\frac{1}{X}\frac{\mathrm{d}X}{\mathrm{d}\xi} = -\frac{q^2}{\ln q}\frac{1}{Q}\frac{\mathrm{d}^2 Q}{\mathrm{d}q^2} (= \beta). \tag{26}$$

The left- and right-hand sides of equation (26) are sole functions of ξ and q, respectively, such that they should be equal to a certain positive constant, denoted above as β. The positive sign of β stems from the increasing solute concentration along the downstream direction, *i.e.*, $\partial\phi/\partial\xi = Q\mathrm{d}X/\mathrm{d}\xi > 0$, as permeation proceeds.

The solution for X in equation (26) is

$$X(\xi) = X_0 \exp\left(\beta K\int_0^\xi \omega^3(\xi')\mathrm{d}\xi'\right), \tag{27}$$

where X_0 is the boundary value of X at the inlet of the membrane channel (*i.e.*, $\xi = 0$), and ξ' is a dummy variable for the integration of $\omega^3(\xi')$. To solve equation (26) for Q, an ansatz is defined:

$$Q = q^n h(q), \tag{28}$$

where n is an arbitrary number to be determined. Substitution of equation (28) into equation (26) provides

$$q^2\frac{\mathrm{d}^2 h}{\mathrm{d}q^2} + 2nq\frac{\mathrm{d}h}{\mathrm{d}q} + \left[\beta\log q + n(n-1)\right]h = 0, \tag{29}$$

which is simplified as

$$\beta^2\frac{\mathrm{d}^2 h}{\mathrm{d}p^2} + (2n-1)\beta\frac{\mathrm{d}h}{\mathrm{d}p} + ph = 0, \tag{30}$$

where

$$p = \beta\ln q + n(n-1). \tag{31}$$

Without losing generality, one can set $n = 1/2$ to eliminate the first-order differential term in equation (30), which is further simplified to

$$\frac{\mathrm{d}^2 h}{\mathrm{d}r^2} = rh, \tag{32}$$

where

$$r = -\frac{p}{\beta^{2/3}} = \frac{\frac{1}{4} - \beta\ln q}{\beta^{2/3}} = \frac{\frac{1}{4} + \beta\,\mathrm{Pe}\,\omega(\xi)\eta}{\beta^{2/3}} > 0. \tag{33}$$

Equation (32) is known as Airy differential equation, and the solution for h is

$$h = \mathrm{Ai}(r) + Q_0\mathrm{Bi}(r), \tag{34}$$

where Ai and Bi are Airy functions, which can be written for $r > 0$ as

$$\mathrm{Ai}(r) = \frac{1}{\pi}\sqrt{\frac{r}{3}}K_{1/3}\left(\frac{2}{3}r^{3/2}\right), \tag{35a}$$

$$\mathrm{Bi}(r) = \sqrt{\frac{r}{3}}\left[I_{-1/3}\left(\frac{2}{3}r^{3/2}\right) + I_{1/3}\left(\frac{2}{3}r^{3/2}\right)\right]. \tag{35b}$$

Here, $I_n(r)$ and $K_n(r)$ are modified Bessel functions of the first and second kind, respectively. Note that r linearly increases with respect to y, having the minimum value of $\frac{1}{4}\beta^{-2/3}$. $\mathrm{Ai}(r)$ and $\mathrm{Bi}(r)$ are decreasing and increasing functions of positive r, respectively, and their asymptotic behaviors with large r are given by

$$\mathrm{Ai}(r) \sim \frac{e^{-\frac{2}{3}r^{3/2}}}{2\sqrt{\pi}r^{1/4}}\,, \tag{36a}$$

$$\mathrm{Bi}(r) \sim \frac{e^{\frac{2}{3}r^{3/2}}}{\sqrt{\pi}r^{1/4}}\,. \tag{36b}$$

One might consider that the coefficient Q_0 of equation (34) must be zero due to the increasing propensity of $\mathrm{Bi}(r)$. It is worth noting that the concentration within the CP layer is bounded between the feed concentration and the wall concentration:

$$C_f < C(x,y) < C_m(x).$$

Above the thin CP layer, concentration is set to be equal to the feed concentration due to the unceasing input of solutes from the feed stream. Although $\mathrm{Bi}(r)$ increases from the membrane surface toward the epicenter of the membrane channel, its contribution to the concentration profile only plays a role in satisfying the boundary condition of equation (7), and by doing so, Q_0 must remain small and the concentration decreases with respect to y (see Fig. 3). Then, the general solution for ϕ within the CP layer is expressed as

$$\phi(\xi,q) = X_0 \exp\left(\beta K \int_0^{\xi} \omega^3(\xi')\mathrm{d}\xi'\right) q^{1/2} \times[\mathrm{Ai}(r) + Q_0\mathrm{Bi}(r)], \tag{37}$$

where X_0, Q_0, and β are unknown constants to be determined.

2.3 Boundary conditions

2.3.1 At the channel inlet

At the inlet of the membrane channel, the concentration must be identical to the feed concentration because the diffusion in the tangential direction is fully neglected in equation (3):

$$\phi(\xi=0,\ q=1) = \frac{C(x=0,\ y=0)}{C_f} = 1, \tag{38}$$

where the condition of $y=0$ implies the absence of the CP layer at the inlet of the membrane channel (*i.e.*, $\delta_p(x=0)=0$). Then, X_0 is calculated as

$$X_0 = \frac{1}{\mathrm{Ai}(r_0) + Q_0\mathrm{Bi}(r_0)}\,, \tag{39}$$

where

$$r_0 = \frac{1}{4\beta^{2/3}}\,. \tag{40}$$

2.3.2 On the membrane surface

Convective and diffusive fluxes in the normal direction are balanced by employing the no-slip boundary condition on the membrane surface:

$$\left[D_0\frac{\partial C}{\partial y} + v_w C\right]_{y=0} = 0, \tag{41}$$

which is equivalent to

$$\left[q\frac{\partial \phi}{\partial q} - \phi\right]_{q=1} = 0 \tag{42}$$

with complete rejection (see the following section). Substitution of equation (37) into equation (42) renders

$$Q_0 = -\frac{\mathrm{Ai}(r_0) + 2\beta^{\frac{1}{3}}\mathrm{Ai}'(r_0)}{\mathrm{Bi}(r_0) + 2\beta^{\frac{1}{3}}\mathrm{Bi}'(r_0)}\,, \tag{43}$$

where the prime superscript indicates differentiation.

2.4 Global mass balance

Global mass balances for solvent and solute are described as

$$Q_f = Q_p + Q_c \tag{44}$$

and

$$C_f Q_f = \langle C_p\rangle Q_p + \langle C_c\rangle Q_c\,, \tag{45}$$

respectively. Here, Q_f, Q_p, and Q_c are the volumetric flow rate of feed, permeate, and concentrate streams, respectively. $\langle C_p\rangle$ and $\langle C_c\rangle$ are length- and height-averaged solute concentrations in the permeate and concentrate streams, respectively. Using equation (44), equation (45) is rewritten in a dimensionless form with the perfect rejection condition (*i.e.*, $\langle C_p\rangle = 0$) as

$$\frac{\langle C_c\rangle}{C_f} = \frac{1}{1-\alpha\langle\omega\rangle}\,, \tag{46}$$

where $\alpha\langle\omega\rangle$ stands for the recovery ratio of the membrane filtration system. The ratio of the height-averaged concentrate concentration to the feed concentration can be calculated as

$$\begin{aligned}\frac{\langle C_c\rangle}{C_f} &= \frac{1}{C_f h}\int_0^h C(x=L,y)\mathrm{d}y \\ &= \int_0^1 \phi(\xi=1,\eta)\mathrm{d}\eta \\ &\equiv \Phi(\omega_f,\omega_1,\beta,\mathrm{Pe}),\end{aligned} \tag{47}$$

where $\omega_1 = \omega(\xi=1)$ is the dimensionless permeate flux at the end of the membrane channel. Then, equation (46) is rewritten for $\langle\omega\rangle$ as

$$\langle\omega\rangle = \frac{1}{\alpha}\left(1 - \frac{1}{\Phi}\right) \tag{48}$$

whose dependence on α is explained as follows. As noted in Section 2.1, terms with α and η^2 ($\eta \ll \eta_p$) are neglected to obtain equation (20), which implies that the spatial variation of the concentration within the CP layer is subject to the unperturbed flow field that satisfies equation (22). Justification of this approach originates from the thinness of the CP layer and the ratio of the length-averaged permeate flux to the height-averaged tangential flow, *i.e.*,

$$\frac{\langle v_w \rangle}{\bar{u}} = \frac{O(10^{-5})\,\mathrm{m/s}}{O(10^{-1})\,\mathrm{m/s}} = O(10^{-4}) \ll 1. \tag{49}$$

On the other hand, it is very important to accurately calculate $\langle C_c \rangle / C_f$ with the pre-determined α of equation (14) because the concentration polariztion resulting in $C_m (> C_f)$ only occurs in the thin CP layer. When the concentration is integrated with respect to η at the end of the membrane channel to calculate the average concentrate concentration (of Eq. (47)), the effect of the biased concentration profile within the thin CP layer is smeared out over the channel height, resulting in $\langle C_c \rangle - C_f$ (much) less than $C_m - C_f$ at $x = L$.

2.5 Osmotic pressure model

2.5.1 Permeate flux

Given a position x, the osmotic pressure affects the permeate flux as follows:

$$v_w = \frac{\Delta P - \Delta \pi_m}{\mu R_m}\,, \tag{50}$$

where μ is the absolute viscosity of the solvent, and R_m is the inherent membrane resistance. Here, $\Delta \pi_m$ is the osmotic pressure difference across the membrane, represented with the complete rejection as

$$\Delta \pi_m = k_b T C_m - 0 = k_b T C_f \phi_m\,, \tag{51}$$

where

$$\phi_m = \phi(\xi, \eta = 0). \tag{52}$$

It is arguable that the osmotic pressure concept can be rigorously applied to such dynamic processes of membrane filtration. A membrane filtration unit is thermodynamically an open system so that the contribution of the osmotic pressure must be diminished to a certain extent in comparison to that in a static equilibrium state [33]. In this study, however, it is assumed that the steady state (of RO processes) can be approximately mimicked by the static equilibrium for solute mass balance [34].

At the inlet of the membrane channel (*i.e.*, $\xi = 0$), the permeate flux is calculated using the feed osmotic pressure as

$$v_{w0} = \frac{\Delta P - k_b T C_f}{\mu R_m}\,. \tag{53}$$

Incorporation of equation (37) into (50) gives

$$\omega(\xi) = \frac{v_w}{v_{w0}} = \frac{1 - \hat{\pi}_f \exp\left(\beta K \int_0^\xi \omega^3(\xi')\mathrm{d}\xi'\right)}{1 - \hat{\pi}_f} \tag{54}$$

and therefore

$$\beta K \int_0^\xi \omega^3(\xi')\mathrm{d}\xi' = \ln\left[1 - (1 - \hat{\pi}_f)\,\omega\right] - \ln \hat{\pi}_f\,, \tag{55}$$

where

$$\hat{\pi}_f = \frac{k_b T C_f}{\Delta P}\,. \tag{56}$$

Equation (55) is an integral equation for w, and therefore its differentiation with respect to ξ yields

$$\beta K \mathrm{d}\xi = -\frac{\mathrm{d}\omega}{\omega^3(\omega_f - \omega)}\,, \tag{57}$$

where

$$\omega_f = \frac{1}{1 - \hat{\pi}_f} (> 1). \tag{58}$$

Integration of both sides of equation (57) provides

$$\beta K \xi = \underbrace{\frac{1}{2\omega_f}\left(\frac{1}{\omega^2} - 1\right)}_{\omega_a} + \underbrace{\frac{1}{\omega_f^2}\left(\frac{1}{\omega} - 1\right)}_{\omega_b} + \underbrace{\frac{1}{\omega_f^3} \ln\left(\frac{\omega_f - \omega}{\omega\,(\omega_f - 1)}\right)}_{\omega_c}, \tag{59}$$

which represents ξ as a function of ω whose inverse relationship can provide a profile of the permeate flux along the membrane channel. The dimensionless mean flux is calculated using equation (57) as

$$\beta K \langle \omega \rangle = \beta K \int_0^1 \omega \mathrm{d}\xi = \frac{1}{\omega_f}\left(\frac{1}{\omega_1} - 1\right) + \frac{1}{\omega_f^2} \ln\left(\frac{\omega_f - \omega_1}{\omega_1(\omega_f - 1)}\right). \tag{60}$$

It is phenomenologically well known that $\omega(\xi)$ decreases with increasing ξ so that $\mathrm{d}\omega/\mathrm{d}\xi$ is always negative along the membrane channel. In addition, the second order derivative, $\mathrm{d}^2\omega/\mathrm{d}\xi^2$, using equation (59) provides interesting results with regard to the inflection of the permeate flux:

$$\left[\frac{\mathrm{d}^2\omega}{\mathrm{d}\xi^2}\right]_{\xi=\xi_{\mathrm{inf}}} = \left[-\beta K \frac{\mathrm{d}\omega}{\mathrm{d}\xi}\right]\left(3\omega_f\omega^2 - 4\omega^3\right) = 0. \tag{61}$$

At the point of inflection, $\xi = \xi_{\mathrm{inf}}$, the corresponding flux is

$$\omega_{\mathrm{inf}} = \frac{3}{4}\omega_f\,, \tag{62}$$

where ξ_{inf} can be calculated using equation (59) with $\omega = \omega_{\mathrm{inf}}$. The practical significance of this inflection analysis is as follows.

If ω_f is greater than $4/3 (= 1.33)$, which implies that the feed osmotic pressure is greater than one fourth of the applied pressure (*i.e.*, $\pi_f > \frac{1}{4}\Delta P$), then the inflection point does not exist in the filtration system because the dimensionless permeate flux is bounded as $0 \le \omega \le 1$.

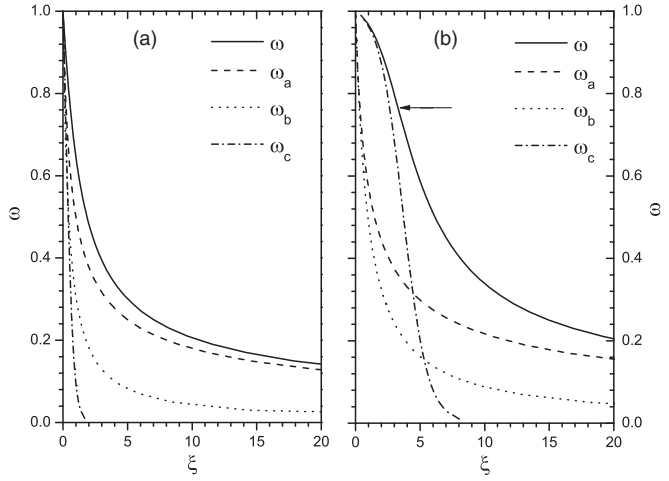

Fig. 2. Variation of the dimensionless permeate flux ω as a function of $\beta K\xi$ with (a) $\omega_f = 1.5$ (*i.e.*, $\Delta P = 3\pi_f$ and $\omega_{\inf} = 1.25$) and (b) $\omega_f = 1.02$ (*i.e.*, $\Delta P = 51\pi_f$ and $\omega_{\inf} = 0.765$). ω_a, ω_b, and ω_c are solely from the first, second, and third components of equation (59), respectively. Note that ω includes the influence of the three components, but graphically $\omega \neq \omega_a + \omega_b + \omega_c$. The components of ω have the following mathematical forms: $\omega_a = (1 + 2\omega_f \beta K\xi)^{-\frac{1}{2}}$, $\omega_b = (1 + \omega_f^2 \beta K\xi)^{-1}$, and $\omega_c = \omega_f/[1 + (\omega_f - 1)e^{\omega_f^3 \beta K\xi}]$.

However, if $\omega_f < 4/3$, meaning that the applied pressure is more than four times the feed osmotic pressure, then the inflection point can be located within the membrane channel, which requires an additional condition of $\omega_1 < \omega_{\inf}$ not to locate the inflection point out of the membrane channel.

Figure 2 shows contributions of each term on the right-hand side of equation (59) (denoted as ω_a, ω_b, and ω_c) to the permeate flux decline. In general, because $\omega_f > 1$ and $\omega < 1$, the first term dominates the second term of equation (59) so that the ω_b curve is always under the ω_a curve. Note that ω_a, ω_b, and ω_c are separately considered in Figure 2 only to express their individual significance on the permeate flux with respect to ξ so that the sum does not represent ω. Variation of ω_c greatly depends on the value of ω_f. If $\omega_f - 1$ has a value of an order of (at least) $O(10^{-1})$ or greater, then the contribution of the logarithmic term of equation (59) is negligible along the membrane channel, as shown in Figure 2(a). In this case, ω_b and ω_c are negligible in comparison to ω_a, which indicates that the permeate flux is inversely proportional to the square root of the distance ξ, *i.e.*,

$$\omega \propto \xi^{-\frac{1}{2}} \tag{63}$$

in an asymptotic manner. Note that the exponent $-\frac{1}{2}$ differs from $-\frac{1}{3}$ from most conventional filtration theories [27] so that the exact solution of equation (59) developed in this study shows a steeper slope of permeate flux decline than predicted by conventional approximations. If $\omega_f - 1$ closely approaches zero, implying that the feed osmotic pressure is negligible compared to the applied pressure, then ω_c dominates over ω_a (which is always greater than ω_b) as long as $\xi \leq \xi_{\inf}$. Note that ω_c almost remains constant for small $\beta K\xi (\ll 1)$ with $\omega_f \to 1^+$. As ξ becomes greater than $\xi_{\inf}$, ω_a gradually becomes dominant as shown in Figure 2(b). Therefore, the presence of $\xi_{\inf}$ in the membrane channel greatly depends on the value of ω_f, which can effectively mitigate the steep, power-wise decline (with the exponent of $-\frac{1}{2}$) of the permeate flux near the channel inlet. Note that the downward concave shape ($\frown$) of Figure 2(b) for small $\beta K\xi$ moves the power-wise decline toward the channel exit, which does not appear in Figure 2(a). Consequently, the inflection point demarcates a phase transition boundary of the permeate flux from the concave-down ($\frown$) to concave-up ($\smile$) regions along the membrane channel, in which ω_c and ω_a are dominant, respectively.

If the feed water does not contain any solute concentration, *i.e.*, $C_f = 0$, then the feed osmotic pressure also vanishes, giving $\omega_f = 1$. In this case, $\Delta P/\Delta\pi_f$ goes to infinity, providing the inflection point located outside the membrane channel. This indicates that permeate flux does not decline in the tangential direction, but converges to Berman's constant suction velocity. Because only a thin CP layer is considered in this study, $\pi_f = 0$ only implies a simple shear flow of solvent on the permeable surface instead of the curvilinear flow within the entire porous channel.

2.5.2 Concentration polarization

Using equation (57), one can solve for X in equation (27):

$$\ln(X/X_0) = \beta K \int_0^{\xi} \omega^3(\xi')\mathrm{d}\xi' = \ln\left(\frac{\omega_f - \omega}{\omega_f - 1}\right). \tag{64}$$

Then, the final solution for the dimensionless concentration is

$$\phi = X_0 \left(\frac{\omega_f - \omega}{\omega_f - 1}\right) \exp\left(-\frac{1}{2}\,\mathrm{Pe}\,\omega\eta\right) \times [\mathrm{Ai}(r) + Q_0 \mathrm{Bi}(r)], \quad \text{for } 0 \leq \eta \leq \eta_p, \tag{65a}$$

$$= 1, \quad \text{for } \eta_p \leq \eta \leq 1, \tag{65b}$$

where

$$\eta_p = \frac{\delta_p}{h} \tag{66}$$

is the dimensionless CP layer thickness. At a given position ξ, the dimensionless wall concentration is then described as

$$\frac{C_m}{C_f} = \phi_m(\xi) = \phi(\xi, q = 1) = \frac{\omega_f - \omega(\xi)}{\omega_f - 1} \tag{67}$$

which shows a linear relationship between the wall concentration and the permeate flux.

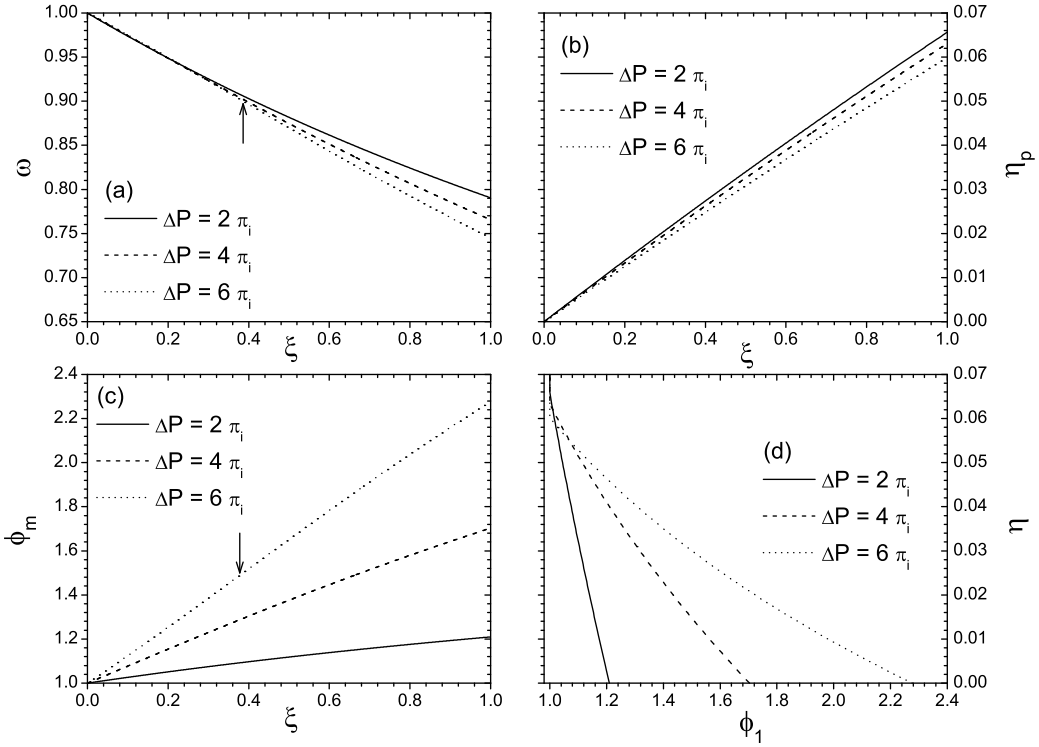

Fig. 3. Effects of pressure on (a) permeate flux ω, (b) CP layer thickness $\eta_p = \delta_p/H$, (c) wall concentration $\phi_m = \phi(\xi, \eta = 0)$, and (d) exit concentration $\phi_1 = \phi(\xi = 1, \eta)$, in dimensionless forms. The parameters used with the above three different applied pressure $\Delta P = 2\pi_f(\mathrm{Re}_{\mathrm{suction}} = 5 \times 10^{-3})$, $4\pi_f(\mathrm{Re}_{\mathrm{suction}} = 1.5 \times 10^{-2})$, and $6\pi_f(\mathrm{Re}_{\mathrm{suction}} = 2.5 \times 10^{-2})$, are: $C_f = 0.1\,\mathrm{M}$, $\gamma_0 = 300\,\mathrm{s}^{-1}$, $L = 0.3\,\mathrm{m}$, $h = 1.0\,\mathrm{mm}$, $R_m = 0.5 \times 10^{14}\,\mathrm{m}^{-1}$, and $D_0 = 1.33 \times 10^{-9}\,\mathrm{m}^2/\mathrm{s}$. The crossflow Reynolds number $\mathrm{Re}_{\mathrm{cross}}$ is 100. Using Van 't Hoff's equation (Eq. (51)), the feed osmotic pressure is calculated as $\pi_f = 248.0\,\mathrm{kPa}$ (= 36.0 psi). The arrows shown in (a) and (c) indicate the inflection location $\xi_{\mathrm{inf}} = 0.386$ for the case of $\Delta P = 6\pi_f$.

2.5.3 Solution procedure

Although all the solutions were derived analytically, an iterative or trial-and-error method is necessary to quantify profiles of the concentration and permeate flux within the CP layer. The procedure is as follows:

1) Assume $\omega_{1,\mathrm{guess}}$ to be between 0 and 1.
2) With K, ω_f, and $\omega_{1,\mathrm{guess}}$, calculate β using equation (59).
3) Calculate $\langle\omega\rangle$ using equation (48).
4) Calculate a returned value of $\omega_{1,\mathrm{return}}$ using equation (60).
5) Set $\omega_{1,\mathrm{guess}}$ as $\omega_{1,\mathrm{return}}$ and return to step (2) until they converge to each other.

3 Results and discussion

3.1 Effects of inflection by applied pressure

Figure 3 shows effects of applied pressure on dimensionless local profiles of permeate flux, CP thickness, wall Figure 3(a) shows that for $\Delta P \leq 4\pi_f$ the permeate flux declines monotonously in a power-wise manner, showing a concave-up profile. (Note $\xi_{\mathrm{inf}} = 0$ for $\Delta P = 4\pi_f$.) For $\Delta P = 6\pi_f$, the inflection of ω occurs at $\xi = 0.386$ as indicated by the upward arrow. The inflection point does not clearly discriminate a curved transition from the concave-down ($0 \leq \xi \leq \xi_{\mathrm{inf}}$) to concave-up ($\xi_{\mathrm{inf}} \leq \xi \leq 1$) region, but it rather makes the permeate flux linear with respect to ξ. Note that Figure 3(a) shows the dimensionless permeate flux ω scaled by the inlet flux v_{w0} which is linearly proportional to the applied pressure so that ω of the highest pressure is at the bottom of the graph.

The dimensionless CP layer thickness η_p is shown in Figure 3(b). Higher pressure causes a thinner CP layer because enhanced convection by higher pressure pushes more solute ions from the bulk phase toward the membrane surface, inducing back diffusion. But, the back diffusion (*i.e.*, an effect), in principle, cannot overcome the enhanced convection (*i.e.*, a cause).

Figure 3(c) shows a dimensionless wall concentration as a function of ξ. Cases of $\Delta P = 2\pi_f$ and $4\pi_f$ show relatively power-wise, curved increases of the wall concentration as expected by Figure 3(a) (using Eq. (67)). The inflection in the $\Delta P = 6\pi_f$ case does not create apparent curved shapes of wall concentrations, but it rather contributes to the linearity of the profile. The value of ϕ_m at $\xi = 1$ for $\Delta P = 6\pi_f$ is about 2.28, which indicates that the actual wall concentration at the end of the membrane channel is 2.28 times greater than the feed concentration, *i.e.*, $C(x = L,\ y = 0) = 2.28 C_f = 0.228\,\mathrm{M}$.

Figure 3(d) shows exit concentration profiles along the axis normal to the membrane surface, and it confirms the

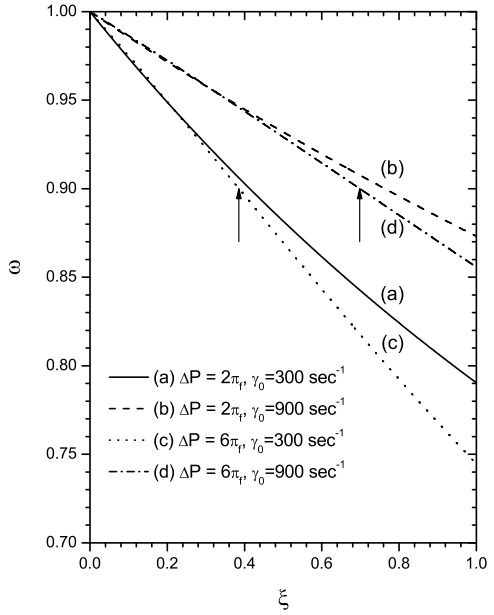

Fig. 4. Effects of shear on the permeate flux ω with $\Delta P = 2\pi_f$ ($\mathrm{Re}_{\mathrm{suction}} = 5 \times 10^{-3}$) and $\Delta P = 6\pi_f$ ($\mathrm{Re}_{\mathrm{suction}} = 2.5 \times 10^{-2}$). Other parameters used in this figure are the same as those of Figure 3. Short-line arrows indicate the inflection location $\xi_{\mathrm{inf}} = 0.386$ and 0.698 for the cases of $\gamma_0 = 300\,\mathrm{s}^{-1}$ ($\mathrm{Re}_{\mathrm{cross}} = 100$) and $900\,\mathrm{s}^{-1}$ ($\mathrm{Re}_{\mathrm{cross}} = 300$), respectively.

findings in Figures 3(a), (b), and (c) from a different view point. In Figure 3(b), η_p values at $\xi = 1$ are the same as η values for $\phi_1 = 1$ in Figure 3(d). Also, ϕ_m values at $\xi = 1$ in Figure 3(c) are identical to ϕ_1 values at $\eta = 0$ in Figure 3(d). Figure 3(d) indicates that a higher pressure generates a more curved CP profile with a higher wall concentration but a smaller CP thickness.

3.2 Effects of wall shear rate

Figure 4 shows that the permeate flux increases with shear rate. This is because a faster crossflow sweeps more solute ions away from the membrane surface downstream, leaving on the membrane surface a lower amount of solutes that can contribute to the osmotic pressure. The absence of the inflection (cases (a) and (b) of Fig. 4) due to the pressure value less than $4\Delta\pi_f$ clearly shows gradual power-wise decline of local permeate flux profiles.

When the inflection occurs (cases (c) and (d) of Fig. 4), the higher shear rates contribute to translation of the inflection position ξ_{inf} toward the membrane channel exit. The permeate flux profile does not have apparent geometrical curvature so that the presence of the inflection points contributes to a linearity of the permeate flux in the tangential direction.

3.3 Comparison to conventional theory

In this section, some of the results shown in Figure 3 are compared to those from the conventional film theory whose basic formalism is summarized as follows. Within the CP layer (the so-called stagnant film layer) the convection is assumed to be balanced with the back-diffusion in the normal direction to the membrane surface, *i.e.*,

$$v_w(x)\phi = -D_0 \frac{\mathrm{d}\phi}{\mathrm{d}y}\,, \tag{68}$$

which completely ignores the convective transport due to the shear flow in the tangential direction. Equation (68) is then integrated across the entire CP layer of thickness $\delta_{p,\mathrm{film}}$ to provide

$$v_w(x) = k(x) \ln\left(\frac{C_m}{C_f}\right), \tag{69}$$

where the local mass transfer coefficent is defined as

$$k(x) \equiv \frac{D_0}{\delta_{p,\mathrm{film}}(x)} \tag{70}$$

and can be approximately evaluated from the analoguos heat transfer analysis [35] as

$$k(x) = 0.538 \left(\frac{D_0^2 \gamma_0}{x}\right)^{1/3}. \tag{71}$$

This mass transfer coefficient only implicitly includes the effect of shear on the normal transport in a crude manner. A major limitation imposed on equation (71) is the assumption that the permeate velocity is constant along the crossflow direction and does not influence the CP layer thickness at all. Nevertheless, a dimensionless CP layer thickness can be obtained using equations (70) and (71):

$$\eta_{p,\mathrm{film}}(\xi) = \frac{\delta_{p,\mathrm{film}}}{h} = \frac{1}{0.538}\left(\frac{D_0 L}{\gamma_0 h^3}\right)^{1/3} \xi^{1/3} \tag{72}$$

as comparable to η_p of the current study. The exponent, $\frac{1}{3}$, of ξ in equation (72) represents only a gradual, power-wise, monotonous increase of $\eta_{p,\mathrm{film}}$ with respect to ξ, which implies that film theory may be a better predictor for low-pressure filtration phenomena.

Length-averaged expressions of equations (71) and (72) are represented as

$$\bar{k} = 0.807 \left(\frac{D_0^2 \gamma_0}{L}\right)^{1/3} \tag{73}$$

and

$$\bar{\eta}_{p,\mathrm{film}} = \frac{1}{0.807}\left(\frac{D_0 L}{\gamma_0 h^3}\right)^{1/3}, \tag{74}$$

respectively, whose values, using the parameters listed in Figure 3, are $\eta_{p,\mathrm{film}}(\xi = 1) = 0.204$ and $\bar{\eta}_{p,\mathrm{film}} = 0.136$. This clearly indicates that film theory provides higher CP layer thickness than that obtained by the current theory and must originate from the following reasons: first, the forceful decoupling of the tangential convection term from the governing mass balance, leading to equation (68), which brings forth an *exponentially* varying concentration profile; and, second, the direct use of the mass transport correlation, developed in a course of heat transfer using impermeable products [35].

The use of the unperturbed flow field satisfying equation (22) and the assumption of the linear shear flow instead of the rigorous parabolic profile over the membrane surface make it possible to derive general analytic forms of concentration and permeation profiles. These approximations may develop a CP layer thinner than a true CP profile due to the overestimated tangential transport away from the membrane surface. From the root origin of the mass transfer coefficient, however, the film theory seems to be less erroneously applied to the following cases: 1) the osmotic pressure is (less than but) comparable to the applied pressure, generating a low permeate flux, and 2) the membrane length is long enough to generate gradual (or negligible) variation of the permeate flux along the tangential direction. Although the film theory is a theoretically rough approach, it is practically useful for system operators who need to estimate the degree of concentration polarization using the mass transfer coefficient and experimentally measured permeate flux using equation (69).

4 Conclusions

The convection-diffusion equation for RO crossflow filtration is analytically solved using four approximations of equations (2–5). The functional transformation and separation of variables are used to provide the general solution of the concentration profile within the CP layer. The osmotic pressure model is used to link the wall concentration and the local permeate flux.

Concentration variation along the normal direction to the membrane surface is attributed to partially power-wise [15,16] and partially exponential [21–23] decay forms as described in equation (65) while solutes are perfectly rejected on the membrane surface. Direct coupling between the concentration and permeate flux gives a unique asymptotic behavior of the permeate flux that is proportional to the inverse square root of the distance in the tangential direction far from the channel inlet, *i.e.*, $v_w \propto x^{-\frac{1}{2}}$.

Applied pressure, which is at least four times greater than the feed osmotic pressure, is the necessary condition to have an inflection of the permeate flux. To locate the inflection point within the membrane channel, the permeate flux at the inflection point should be greater than the exit permeate flux. The presence of the inflection point within the membrane channel mitigates the steep power-wise flux decline by generating the concave-down variation of the flux near the channel inlet. The curvature effect at the inflection point is, however, usually not apparent. Instead, the inflection modifies the flux decline behavior from a power-wise to a phenomenologically linear form. The present analytic solution is more accurate when a fast crossflow is imposed in a short membrane channel, confirming the negligible α.

This research was made possible by a grant from the US National Science Foundation Faculty Early Career (CAREER) Development Program (CTS04-49431).

Appendix A. An asymptotic analysis: a formal expansion

This section proves that the tangential diffusion is minimal in comparison to the other three transport terms, *i.e.*, tangential convection, normal convenction and diffusion. Typically in crossflow membrane filtration, it is assumed that the crossflow velocity is much faster than the permeate flux, and that the length is much longer than the channel height, *i.e.*, $\bar{u} \gg v_{w0}$ and $L \gg h$, respectively. The concentration polarization caused by rejection of solute ions under the influence of the permeate flux v_{w0} is therefore considered just a perturbation relative to the tangential convective transport. The following cases are carefully considered for this comparative asymptotic analysis.

Case A: The membrane is impermeable to the solvent, and the solute is absent: $(u, v) = (\gamma_0 y, 0)$ and $C = 0$.

Case B: The membrane is impermeable to the solvent, and the solute is present: $(u, v) = (\gamma_0 y, 0)$ and $C \simeq C_f$.

Case C: The membrane is permeable to the solvent, and the solute is absent:

$$(u, v) = \left(\gamma_0 y + \epsilon^a u_1, \epsilon^b v_1\right) \tag{A.1}$$

and $C = 0$, where $\epsilon(\ll 1)$ is the perturbation parameter, and a and b are arbitrary positive constants. The magnitude of u_1 and v_1 is of similar order to u, *i.e.*, $O(u) \sim O(u_1) \sim O(v_1)$. This case is therefore within the regime of Berman's perturbation solution [1] for a laminar flow over a porous wall with a small suction Reynolds number as in equation (23).

Case D: This case is a combination of Case B and C by applying to Case A the perturbed flow field (Eq. (A.1)) and the nonzero solute concentration, $C \gtrsim C_f$. Using the flow field, the continuity equation (Eq. (6)) is rewritten in a dimensionless form as

$$\frac{\epsilon^a}{L}\frac{\partial \hat{u}_1}{\partial \xi} + \frac{\epsilon^b}{h}\frac{\partial \hat{v}_1}{\partial \eta} = 0\,, \tag{A.2}$$

where $(\hat{u}_1, \hat{v}_1) = (u_1/\bar{u}, v_1/\bar{u})$. Equation (A.2) indicates

$$\epsilon^{a-b} \sim \frac{L}{h} \gg 1 \tag{A.3}$$

and so

$$a - b < 0. \tag{A.4}$$

The perturbation terms of equation (1) are collected as

$$\frac{\partial \hat{u}_1 \phi}{\partial \xi} + \frac{\partial \hat{v}_1 \phi}{\partial \eta} \simeq \frac{D_0}{\bar{u}L}\epsilon^{-a}\left(\frac{\partial^2 \phi}{\partial \xi^2} + \epsilon^{2(a-b)}\frac{\partial^2 \phi}{\partial \eta^2}\right) \tag{A.5}$$

while the unperturbed contribution is close to Case B. Using equation (A.3), equation (A.5) proves that the tangential diffusion is negligible relative to the normal diffusion. The weight factor of the tangential diffusion further shows

its minute significance in comparison to tangential and normal convection using $v_{w0}/\bar{u} \sim \epsilon^b$ from equation (A.1):

$$\frac{D_0}{\bar{u}L}\epsilon^{-a} = \left(\frac{D_0}{v_{w0}h}\right)\left(\frac{v_{w0}}{\bar{u}}\right)\left(\frac{h}{L}\right)\epsilon^{-a} \simeq \mathrm{Pe}^{-1}\,\epsilon^{-2(a-b)} \tag{A.6}$$

since $\epsilon^{-2(a-b)} \ll 1$. Note that the magnitude of the Peclet number, Pe, is roughly

$$O(\mathrm{Pe}) = O\left(\frac{v_{w0}h}{D_0}\right) = \frac{O(10^{-6})O(10^{-3})}{O(10^{-9})} = O(1) \tag{A.7}$$

in reverse osmosis and nanofiltration processes. The tangential diffusion becomes as important as the normal diffusion only if $a \sim b$, indicating $h \sim L$, which is not realistic in any crossflow filtration. The magnitude of α (of Eq. (14)), presumed to be negligible, is reconfirmed as

$$\alpha = \frac{v_{w0}}{2\bar{u}}\frac{L}{h} \sim \epsilon^b\epsilon^{a-b} = \epsilon^a \tag{A.8}$$

which is consistent with equation (5) and (A.1). The final asymptotic form of equation (A.5) is then

$$\frac{\partial \hat{u}_1\phi}{\partial\xi} + \frac{\partial \hat{v}_1\phi}{\partial\eta} \simeq \frac{1}{\mathrm{Pe}}\frac{\partial^2\phi}{\partial\eta^2} \tag{A.9}$$

which represents the solute transport, convoluted with Berman's perturbed flow field and later the osmotic pressure contribution. Above the CP layer ($y > \delta_p$), equation (A.9) returns to the continuity equation of equation (A.2):

$$\frac{\partial \hat{u}_1}{\partial\xi} + \frac{\partial \hat{v}_1}{\partial\eta} \simeq 0 \tag{A.10}$$

which is valid throughout the entire membrane channel.

References

1. A.S. Berman, J. Appl. Phys. **24**, 1232 (1953).
2. R.D. Bundy, H.L. Weissberg, Phys. Fluids **13**, 2613 (1970).
3. H.L. Weissberg, Phys. Fluids **2**, 510 (1959).
4. M. Morduchow, Q. J. Appl. Math. **14**, 361 (1956).
5. J.F. Brady, Phys. Fluids **27**, 1061 (1984).
6. L. Durlofsky, J.F. Brady, Phys. Fluids **27**, 1068 (1984).
7. G.S. Beavers, D.D. Joseph, J. Fluid Mech. **30**, 197 (1967).
8. G. Taylor, J. Fluid Mech. **49**, 319 (1971).
9. J.T. Jeong, Phys. Fluids **13**, 1884 (2001).
10. S. Chellam, M. Liu, Phys. Fluids **18**, 083601 (2006).
11. A.S. Michaels, Chem. Eng. Prog. **64**, 31 (1968).
12. V. Gekas, B. Hallstrom, J. Membrane Sci. **30**, 153 (1987).
13. A.L. Zydney, J. Membrane Sci. **130**, 275 (1997).
14. S.S. Sablani, M.F.A. Goosen, R. Al-Belushi, M. Wilf, Desalination **141**, 269 (2001).
15. D.R. Trettin, M.R. Doshi, Ind. Eng. Chem. Fundam. **19**, 189 (1980).
16. D.R. Trettin, M.R. Doshi, Chem. Eng. Commun. **4**, 507 (1980).
17. J.J.S. Shen, R.F. Probstein, Ind. Eng. Chem. Fundam. **16**, 495 (1977).
18. R.H. Davis, J.D. Sherwood, Chem. Eng. Sci. **45**, 3203 (1990).
19. S.S. Vasan, R.W. Field, J. Membrane Sci. **279**, 434 (2006).
20. S. De, S. Bhattacharjee, A. Sharma, P.K. Bhattacharya, J. Membrane Sci. **130**, 99 (1997).
21. L.F. Song, M. Elimelech, J. Chem. Soci. Faraday Trans. **91**, 3389 (1995).
22. L. Song, J. Membrane Sci. **144**, 173 (1998).
23. L. Song, J. Colloid Interface Sci. **214**, 251 (1999).
24. C.A. Romero, R.H. Davis, J. Membrane Sci. **39**, 157 (1988).
25. C.A. Romero, R.H. Davis, Chem. Eng. Sci. **45**, 13 (1990).
26. S. Kim, E.M.V. Hoek, Desalination **186**, 111 (2005).
27. P. Bacchin, J. Membrane Sci. **228**, 237 (2004).
28. H.M. Yeh, T.W. Cheng, J. Membrane Sci. **154**, 41 (1999).
29. J.P. Hansen, I.R. McDonald, *Theory of Simple Liquids* (Academic Press, London, 1976).
30. G. Eng, Phys. Rev. B **39**, 1518 (1989).
31. R.H. Davis, D.T. Leighton, Chem. Eng. Sci. **42**, 275 (1987).
32. R.H. Davis, Sep. Purif. Methods **21**, 75 (1992).
33. S. Bhattacharjee, A.S. Kim, M. Elimelech, J. Colloid Interface Sci. **212**, 81 (1999).
34. M. Mulder, *Basic Principles of Membrane Technology* (Kluwer Academic Publishers, Boston, Mass., 1996).
35. M.A. Leveque, Ann. Mines **13**, 201 (1928).